Pro-apoptotic activity of inhibitory PAS domain protein (IPAS), a negative regulator of HIF-1, through binding to pro-survival Bcl-2 family proteins

S Torii[1], Y Goto[1], T Ishizawa[1], H Hoshi[1], K Goryo[1], K Yasumoto[1], H Fukumura[2] and K Sogawa*,[1]

Inhibitory PAS (Per/Arnt/Sim) domain protein (IPAS) is a dominant negative transcription factor that represses hypoxia-inducible factor 1 (HIF-1) activity. In this study, we show that IPAS also functions as a pro-apoptotic protein through binding to pro-survival Bcl-2 family members. In a previous paper, we reported that NF-κB-dependent IPAS induction by cobalt chloride repressed the hypoxic response in PC12 cells. We found that prolonged incubation under the same conditions caused apoptosis in PC12 cells. Repression of IPAS induction protected cells from apoptosis. Furthermore, knockdown of IPAS recovered cell viability. EGFP-IPAS protein was localized in both the nucleus and the cytoplasm, with a large fraction associated with mitochondria. Mitochondrial IPAS induced mitochondria depolarization and caspase-3 activation. Immunoprecipitation assays revealed that IPAS is associated with Bcl-x$_L$, Bcl-w and Mcl-1. The association of IPAS with Bcl-x$_L$ was also observed in living cells by the FLIM-based FRET analysis, indicating direct binding between the two proteins. IPAS contributed to dysfunction of Bcl-x$_L$ by inhibiting the interaction of Bcl-x$_L$ with Bax. These results demonstrate that IPAS functions as a dual function protein involved in transcription repression and apoptosis.

Hypoxia-inducible factor 1 (HIF-1) is a transcription factor that functions as a master regulator of gene expression in response to hypoxia.[1–3] HIF-1 consists of an oxygen-regulated HIF-1α subunit and a constitutively expressed Arnt (HIF-1β) subunit. In normoxia, HIF-1α is rapidly degraded by the ubiquitin–proteasome system. On the other hand, in hypoxia, HIF-1 is stabilized, translocated into the nucleus and bound to hypoxia-response element (HRE) to induce downstream gene expression of hypoxia-responsive proteins, such as erythropoietin, vascular endothelial growth factor and tyrosine hydroxylase. The inhibitory PAS (Per/Arnt/Sim) domain protein (IPAS), one of the alternatively spliced variants of HIF-3α, functions as a dominant negative inhibitor of HIF-1.[4] IPAS directly interacts with HIF-1α and HIF-1α-like factor (HLF, also known as HIF-2α or EPAS1) and prevents their dimerization with Arnt and subsequent DNA binding. IPAS is predominantly expressed in the Purkinje cells of the cerebellum and corneal epithelium. In addition, it is reported that IPAS is induced by hypoxia in the heart and lung through activation of HIF-1.[5] Thus, IPAS functions as a negative feedback inhibitor of HIF-dependent hypoxic response.

Hypoxic cell death can be mediated by HIF-1.[6] It can induce apoptosis through activation of BNIP3 and Noxa, which were identified as HIF-1-responsive pro-apoptotic proteins.[7,8] However, HIF-1 also functions to prevent cell death and even stimulate cell proliferation.[9] Constitutive HIF-1 stabilization is observed in many types of cancers, in which it is associated with resistance to hypoxic apoptosis.[9] Recent papers have shown that some anti-apoptotic molecules are identified as HIF-1 targets, such as Bcl-x$_L$ and Mcl-1.[10,11] Although it is considered that a delicate balance determines cell fate between self-killing of cells by apoptosis via induction of pro-apoptotic factors and adaptation of cells to the hypoxic environment through induction of anti-apoptotic factors and cell growth-related proteins, the complex roles of HIF-1 in cell death and cell survival are not fully understood and remain to be elucidated.

Hypoxic cell death is influenced by the presence of reactive oxygen species (ROS). ROS are known to accumulate after ischemic/hypoxic reoxygenation or intermittent hypoxia leading to extensive cell death.[12,13] This situation is observed in several pathophysiological conditions such as cerebral and myocardial infarction.[13,14] Although the role of ROS in cell death is not well understood, they can attack and oxidize nucleic acids, proteins and lipids, resulting in neuronal apoptosis.[13,15]

Rat pheochromocytoma-derived PC12 cells are widely used as *in vitro* model cells for investigating neuronal apoptosis in hypoxia/ischemic conditions.[16–19] There are several reports showing that cobalt chloride (CoCl$_2$) or nitric oxide could mimic hypoxia/ischemic conditions, including generation of ROS, and induces mitochondria damage and

[1]Department of Biomolecular Sciences, Graduate School of Life Sciences, Tohoku University, Aoba-ku, Sendai 980-8578, Japan and [2]Department of Chemistry, Graduate School of Science, Tohoku University, Aoba-ku, Sendai 980-8578, Japan

*Corresponding author: K Sogawa, Department of Biomolecular Sciences, Graduate School of Life Sciences, Tohoku University, Aoba-ku, Sendai 980-8578, Japan. Tel: + 81 22 795 6590; Fax: + 81 22 795 6594; E-mail: sogawa@m.tohoku.ac.jp

apoptosis.[16–20] Recent reports have shown that $CoCl_2$-induced ROS leads to accumulation of HIF-1α in many mammalian cells, including PC12 cells.[21–23] Moreover, our recent report showed that $CoCl_2$-induced ROS also upregulates the expression of IPAS mRNA through NF-κB activation in PC12 cells.[23] Although there is increasing evidence

suggesting a close relationship between hypoxic cell death and ROS generation in hypoxia as described above, the underlying mechanism linking them is not fully understood.

Our analyses here demonstrate that IPAS functions as a pro-apoptotic factor acting in the mitochondria, although it is also localized in the nucleus. We also show that IPAS directly
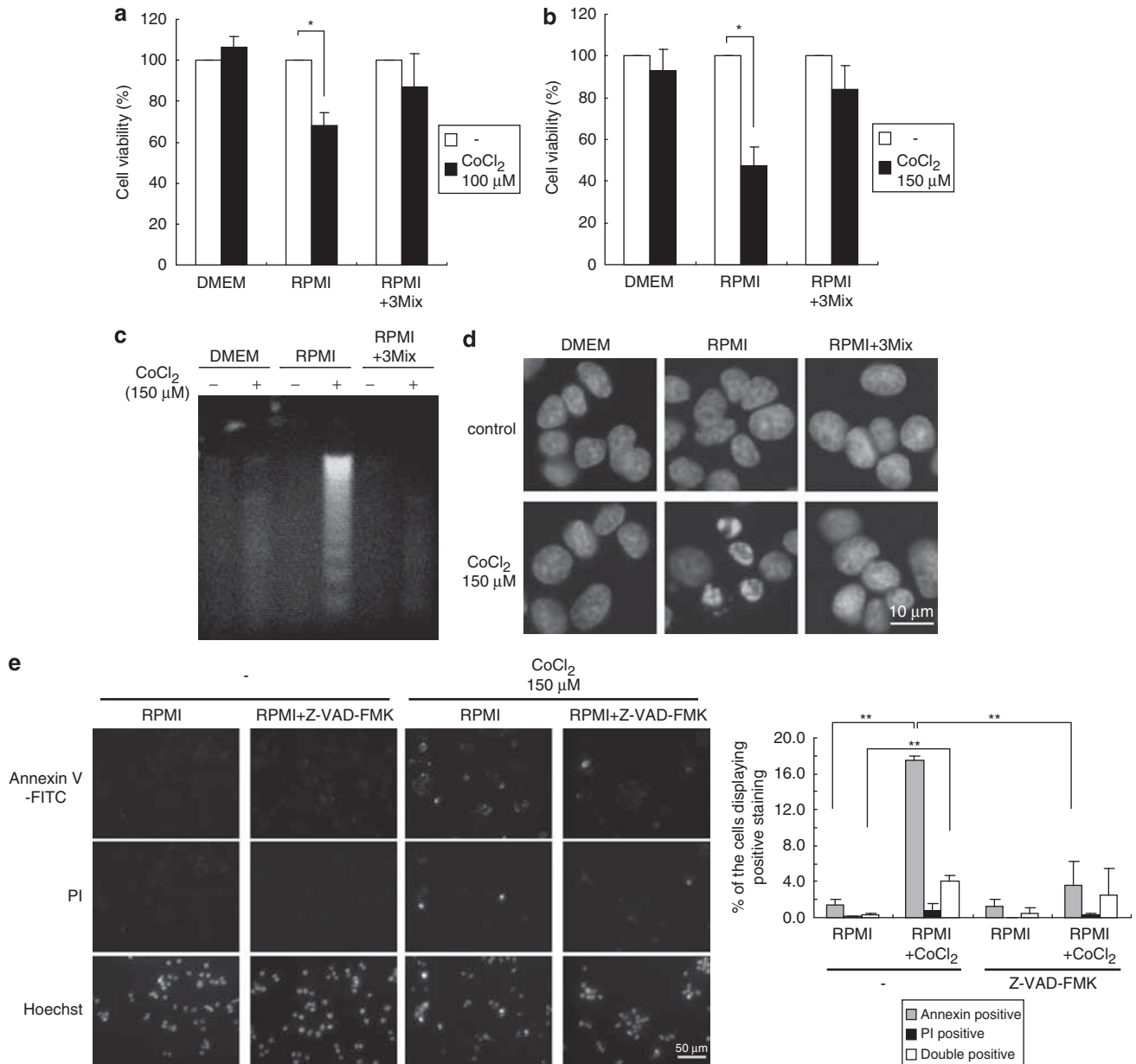
Figure 1 Cell apoptosis induced by $CoCl_2$ in RPMI-cultured PC12 cells. (**a** and **b**) Cell viability was assayed by trypan blue dye exclusion. Cells were incubated in the indicated medium for 24 h with 100 μM (**a**) or 150 μM (**b**) $CoCl_2$. 3Mix indicates a mixture of magnesium, histidine and threonine, giving equivalent concentrations to those included in DMEM. (**c**) $CoCl_2$-induced DNA fragmentation in RPMI-cultured PC12 cells. DNA was prepared from PC12 cells treated with 150 μM $CoCl_2$ for 16 h. (**d**) $CoCl_2$-induced chromatin condensation in RPMI-cultured PC12 cells. Cells were treated with or without 150 μM $CoCl_2$ for 16 h, and stained with Hoechst 33342. (**e**) Annexin V/PI staining of RPMI-cultured PC12 cells. Cells were treated with or without 150 μM $CoCl_2$ in the presence of 20 μM Z-VAD-FMK for 16 h, and stained with Annexin V-FITC and PI (left). Quantification of apoptotic and necrotic cells is expressed as the percentage of the cells displaying Annexin V and Annexin V/PI-double staining, respectively. A minimum of 700 cells per sample was counted and the percentage of cells with respective staining patterns was shown in a bar graph (right). (**f**) Cytochrome *c* staining of PC12 cells. Cells were incubated in the indicated medium for 16 h with or without 150 μM $CoCl_2$. A minimum of 400 cells per sample was counted. Arrowheads: cells with release of cytochrome *c*. (**g**) Active caspase-3 staining of PC12 cells. Cells were incubated in the indicated medium for 16 h with or without 150 μM $CoCl_2$. A minimum of 400 cells per sample was counted. (**h**) Immunoblot analysis of active caspase-3. Cells were incubated in the indicated medium for 16 h with or without 150 μM $CoCl_2$. Cell lysates were analyzed by immunoblotting for the cleavage of caspase-3. Data shown in bar graphs are averages ± S.D. of three independent experiments. *$P < 0.05$ for indicated comparison. **$P < 0.01$ for indicated comparison
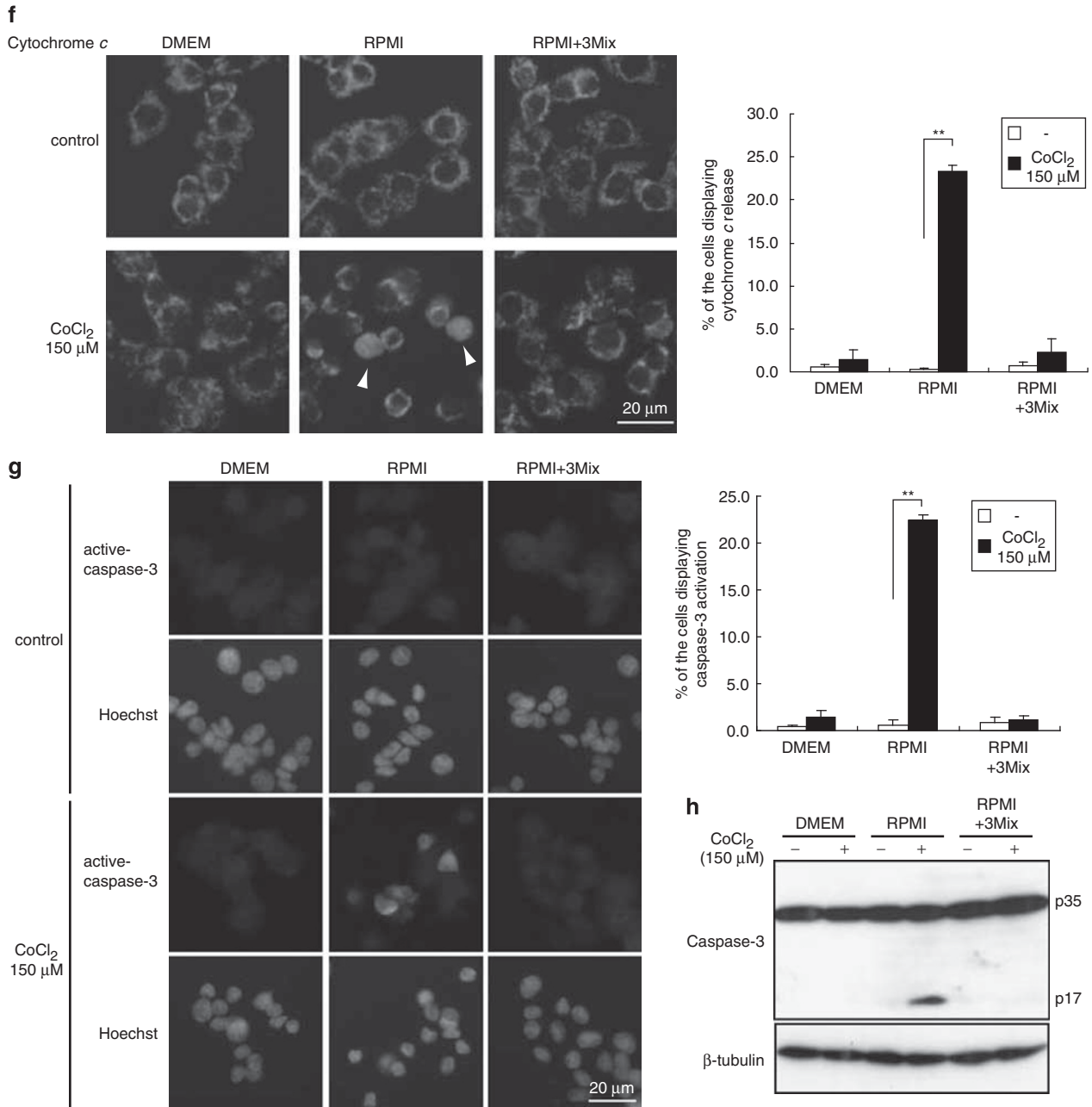
f

g

h

Figure 1 Continued

interacted with pro-survival Bcl-2 family members, such as Bcl-x$_L$, and this binding led to dysfunction of Bcl-x$_L$ by blocking its anti-apoptotic activity to bind to Bax. These results demonstrate that IPAS functions as a dual function protein involved in gene regulation in response to hypoxia and hypoxic apoptosis.

Results

Apoptosis induced by CoCl$_2$ in RPMI-cultured PC12 cells. To examine CoCl$_2$-induced cell death in PC12 cells under different nutritional conditions, PC12 cells were cultured in DMEM or RPMI in the presence of CoCl$_2$ for 24 h, and cell viability was measured by trypan blue exclusion. Figures 1a and b show that CoCl$_2$-induced cell death in PC12 cells occurred when cultured in RPMI medium depending on the concentration of CoCl$_2$, but not at all in DMEM. We have previously shown that IPAS was induced by CoCl$_2$ in PC12 cells when cultured in RPMI but not in DMEM, and that addition of three nutrients, magnesium, histidine and threonine (3Mix) to RPMI abolished the induction.[23] CoCl$_2$-induced cell death in PC12 cells found in RPMI medium was similarly blocked by the addition of 3Mix (Figures 1a and b). Hereafter 150 μM CoCl$_2$ was used to induce cell death because of its potent effect. To determine

whether CoCl$_2$-induced cell death of RPMI-cultured PC12 cells had the characteristics of apoptosis, we carried out DNA fragmentation assay and nuclear staining with Hoechst 33342. DNA fragmentation assay showed that a clear DNA ladder was observed 16 h after exposure of PC12 cells to CoCl$_2$ (Figure 1c) only when cultured in RPMI. Nuclear condensation was detected in CoCl$_2$-treated PC12 cells when cultured in RPMI, but not in DMEM or RPMI with 3Mix (Figure 1d). In addition, Annexin-V/propidium iodide (PI) staining showed that CoCl$_2$ induced apoptosis rather than necrosis, and this cell death was inhibited by a caspase inhibitor, Z-VAD-FMK (Figure 1e). Furthermore, release of mitochondrial cytochrome *c* and activation of caspase-3 were observed in CoCl$_2$-treated PC12 cells when cultured in RPMI (Figures 1f–h).

Induction of IPAS in RPMI-cultured PC12 cells and its role in induction of apoptosis. We have already shown that IPAS expression was significantly induced in response to CoCl$_2$ only when PC12 cells were cultured in RPMI (Figure 2a).[23] Therefore, we hypothesized that IPAS was one of the causal factors in CoCl$_2$-induced apoptosis in RPMI-cultured PC12 cells, and we investigated this possibility by the treatment of PC12 cells with siRNA for IPAS. We have already shown that the endogenous IPAS mRNA level was decreased by IPAS/HIF-3α siRNA treatment (Figure 2b).[23] Downregulation of HIF-3α expression by the treatment was hardly detectable as it was very weakly expressed (Figure 2b). In addition, ectopic expression of Myc-tagged mouse IPAS was greatly decreased following IPAS/HIF-3α siRNA treatment (Figure 2c). IPAS/HIF-3α siRNA treatment
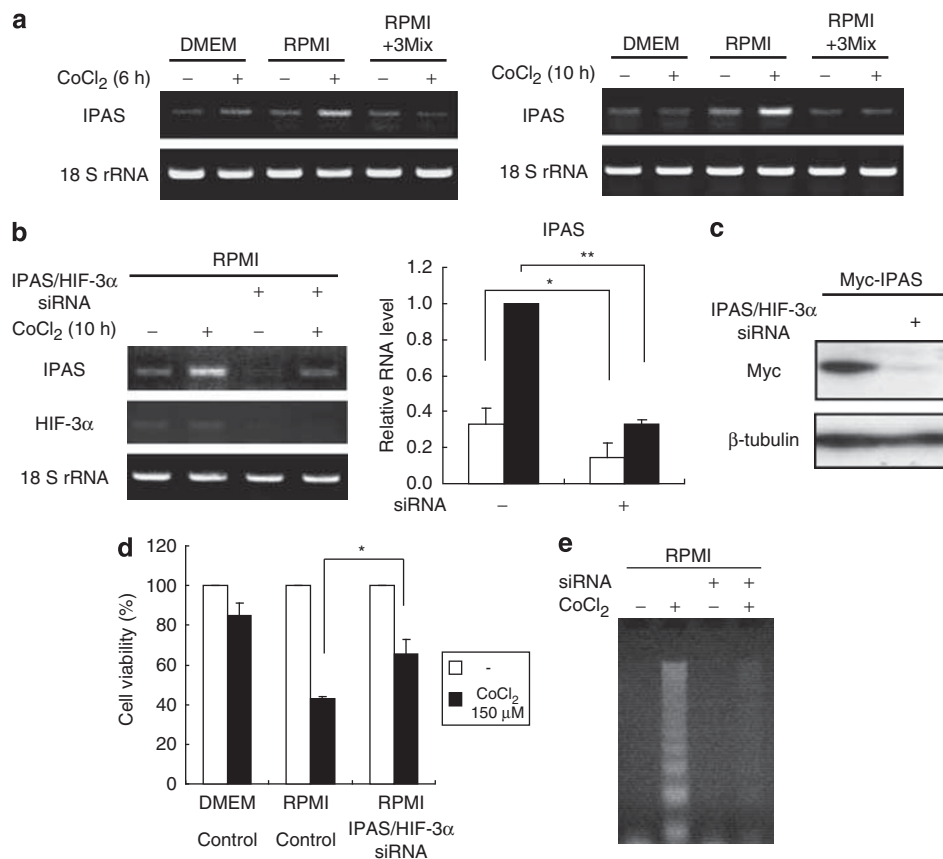
Figure 2 Induction of IPAS by CoCl$_2$ in RPMI-cultured PC12 cells and its involvement in CoCl$_2$-induced apoptosis. (**a**) Time dependence of IPAS mRNA expression in CoCl$_2$-treated PC12 cells cultured in different media. IPAS mRNA expression levels in PC12 cells treated with CoCl$_2$ for 6 h (left) and 10 h (right) were determined by RT-PCR. PCR products were analyzed on 1% agarose gels. 18 S rRNA was used as a control. Data shown are representative of three independent experiments. (**b**) Decrease in IPAS expression by siRNA treatment. GFP siRNA was used as a control. Data were normalized to 18 S rRNA and the value of cells treated with CoCl$_2$ in the presence of GFP siRNA was set to 1. (**c**) Decrease in overexpressed IPAS by siRNA treatment. PC12 cells were transfected with a plasmid for Myc-tagged mouse IPAS and treated with GFP siRNA or IPAS/HIF-3α siRNA for 24 h. Cell lysates were analyzed by immunoblot. β-tubulin was used as a control. (**d**) Cell viability recovered by the treatment with IPAS/HIF-3α siRNA in RPMI-cultured PC12 cells. PC12 cells were transfected with siRNA for 24 h, and incubated in indicated medium in the presence or absence of 150 μM CoCl$_2$ for 24 h. GFP siRNA was used as a control. *$P < 0.05$ for indicated comparison. Data shown in bar graphs are averages ± S.D. of three independent experiments. (**e**) Decrease in CoCl$_2$-induced DNA fragmentation by the treatment with IPAS/HIF-3α siRNA. PC12 cells were transfected with siRNA for 24 h and then incubated in indicated medium in the presence or absence of 150 μM CoCl$_2$ for 16 h. Data shown are representative of three independent experiments. (**f**) Decrease in CoCl$_2$-dependent mitochondrial depolarization by IPAS/HIF-3α siRNA treatment. PC12 cells were transfected with indicated siRNA and incubated with or without CoCl$_2$ for 16 h and stained with JC-1 for 20 min. After washing with RPMI, the cells were observed using a fluorescence microscope. (**g**) Decrease in cytochrome *c* release by IPAS/HIF-3α siRNA treatment. siRNA-transfected cells were incubated in RPMI with or without 150 μM CoCl$_2$ in the presence of Z-VAD-FMK for 16 h. A minimum of 400 cells per sample was counted. Arrowheads show the cells with release of cytochrome *c*. (**h** and **i**) Decrease in activation of caspase-3 by IPAS/HIF-3α siRNA treatment. siRNA-transfected cells were incubated in RPMI with or without 150 μM CoCl$_2$ for 16 h. A minimum of 400 cells per sample was counted (**h**). Cell lysates were analyzed by immunoblotting for the cleavage of caspase-3 (**i**). Data shown in bar graphs are averages ± S.D. of three independent experiments. *$P < 0.05$ for indicated comparison. **$P < 0.01$ for indicated comparison
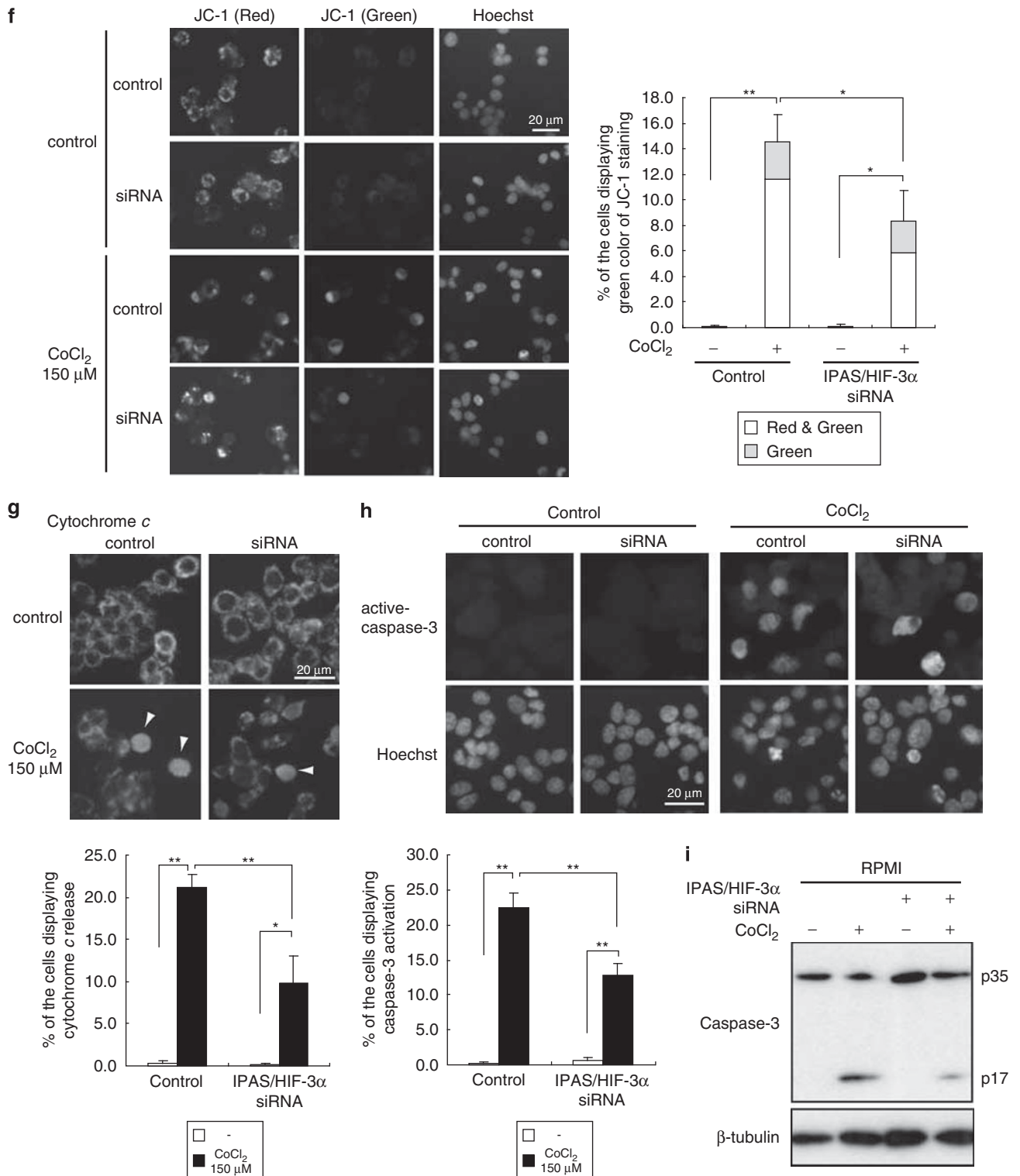
Figure 2 Continued

significantly recovered the cell viability of RPMI-cultured PC12 cells (Figure 2d) and decreased the genomic DNA fragmentation of PC12 cells exposed to CoCl$_2$ (Figure 2e). Next, we examined the effect of siRNA treatment on

mitochondrial membrane potential by JC-1 dye. In non-apoptotic cells, most of the JC-1 accumulated as aggregates in the mitochondria (red fluorescence) and only a small part of the JC-1 localized in the cytoplasm as a monomer (green
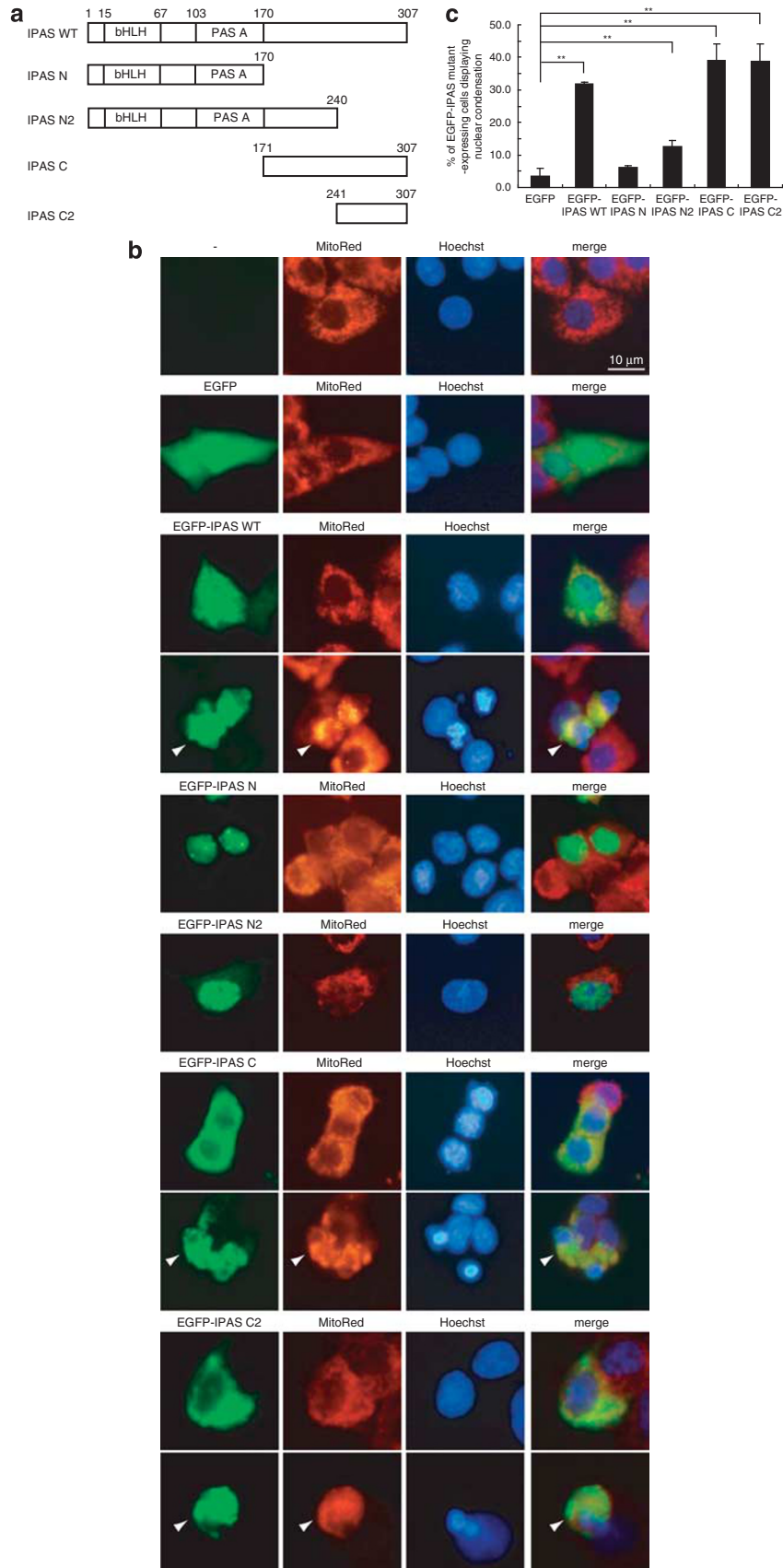
fluorescence) as shown in Figure 2f. Green fluorescence of JC-1 was enhanced by $CoCl_2$ treatment and the siRNA treatment inhibited this enhancement (Figure 2f). Furthermore, release of mitochondrial cytochrome *c* and activation of caspase-3 were inhibited in the cells by the siRNA treatment (Figures 2g and h). Immunoblot analysis also revealed that the siRNA treatment resulted in a significant reduction in the cleaved and active form of caspase-3 (Figure 2i).

Induction of mitochondrial clustering and nuclear condensation due to mitochondrial localization of IPAS. To examine the role of IPAS in $CoCl_2$-induced apoptosis, we constructed a EGFP-tagged IPAS (IPAS WT) expression plasmid together with *C*-terminal deletion (IPAS N and N2) plasmids and two *N*-terminal deletion (IPAS C and IPAS C2) plasmids as shown in Figure 3a, and transfected them into PC12 cells (Figures 3 and 4), human embryonic kidney (HEK) 293T cells (Supplementary Figures 1, 2a and b) and Chinese hamster ovary (CHO)-K1 cells (Supplementary Figure 2c). MitoRed was used to reveal mitochondrial morphology. IPAS WT was localized in both the nucleus and cytoplasm with different nuclear to cytoplasmic ratios for each cell (Figures 3b and 4a and Supplementary Figures 1a and 2). Moreover, IPAS WT induced mitochondrial clustering near the nucleus and nuclear condensation of PC12 cells (Figures 3b and c) and HEK293T cells (Supplementary Figures 1a and b). Further investigation of the cytoplasmic localization with the caspase inhibitor using a confocal microscope showed that IPAS WT was localized in the mitochondria (Figure 4b). Mitochondrial clustering due to IPAS was diminished by the caspase inhibitor in PC12 cells (Figure 4b), indicating that this effect on mitochondrial morphology due to IPAS is downstream of caspase activation and is therefore a consequence of cell death and the condensation of the cell. Nuclear localization of IPAS WT was confirmed by colocalization of PI staining using a confocal microscope (Figure 4c). IPAS N was exclusively localized in the nucleus (Figures 3b, 4a and b, and Supplementary Figures 1a, 2a and b). IPAS N2 was mainly localized in the nucleus. On the other hand, IPAS C colocalized with MitoRed and strongly induced perinuclear mitochondrial clustering, especially in HEK293T cells. IPAS C2 was diffusely localized in the cytoplasm, partially colocalized with MitoRed and induced mitochondrial clustering to some extent (weaker in the effect than WT and C). IPAS C and C2 induced nuclear condensation of PC12 cells (Figure 3c) and HEK293T cells (Supplementary Figure 1b). IPAS N did not induce nuclear condensation. IPAS N2 induced nuclear abnormality to a much lower extent in PC12 cells.

Mitochondrial depolarization, release of cytochrome *c* and activation of caspase-3 induced by IPAS. To determine whether mitochondrial localization of IPAS initiates intracellular apoptosis signaling, we examined mitochondrial membrane potential by JC-1 fluorescent staining, release of cytochrome *c* and activation of caspase-3. When Cerulean-IPAS WT was expressed in PC12 cells, the percentage of cells exhibiting green fluorescence was enhanced (Figure 5a). When Cerulean-IPAS C was expressed, green fluorescence was observed in about 25% of PC12 cells (Figure 5a), suggesting that IPAS C was the more powerful inducer of mitochondrial depolarization. IPAS C2 induced mitochondrial depolarization to a similar extent as IPAS WT. IPAS N was unable to induce depolarization of mitochondria (Figure 5a). Next, we investigated release of cytochrome *c* in IPAS-expressed cells. IPAS WT, C and C2, but not IPAS N, induced release of cytochrome *c* in PC12 cells (Figure 5b). Ability of IPAS-deletion mutants to release cytochrome *c* was associated with their activity to induce depolarization of mitochondrial membranes. High levels of active caspase-3 were observed in the cells expressing IPAS WT, C and C2, whereas IPAS N was unable to activate caspase-3 (Figure 6 and Supplementary Figure 3).

Specific binding of IPAS to pro-survival Bcl-2 family proteins through its C-terminal region and inhibition of Bcl-x_L/Bax complex formation by IPAS. The possibility was considered that IPAS might inhibit the function of Bcl-2 family proteins. To test this possibility, binding between IPAS and Bcl-2 family members was examined. Immunoprecipitation experiments in HEK293T cells showed that IPAS was able to bind to Bcl-x_L, but not to Bcl-2 and Bax (Figure 7a). Similar results were obtained in the presence of Z-VAD-FMK (Supplementary Figure 4a). When Bcl-2 was highly expressed, a modest interaction with IPAS was observed (Supplementary Figure 4b). In addition, ectopically expressed IPAS was bound to endogenous Bcl-x_L, but not to Bcl-2 and Bax (Figures 7b and c). Next, we examined whether IPAS binds to other pro-survival Bcl-2 family members. Figure 7d shows that IPAS bound to Bcl-x_L, Bcl-w and Mcl-1 variant (Mcl-1V) with similar affinity, but not to Bcl-2 and A1a (also known as A1/Bfl-1). The C-terminal region of IPAS was found to interact with Bcl-x_L whereas the N-terminal region did not interact with Bcl-x_L (Figure 7e). This result accords well with the apoptotic activity of the C-terminal region (Figures 5 and 6 and Supplementary Figure 3). Although binding of IPAS C2 to Bcl-x_L was examined, Myc-IPAS C2 was not detected in the cell lysate when Bcl-x_L was co-expressed, possibly due to degradation because of its shorter tag. We investigated subcellular localization of IPAS and Bcl-x_L using confocal fluorescent microscopy to examine their colocalization. Although Bcl-x_L

Figure 3 Induction of mitochondria clustering and nuclear condensation due to IPAS expression. (**a**) Schematic representation of the N- and C-terminal regions of IPAS used for plasmid construction. bHLH: basic helix-loop-helix domain; PAS: Per/Arnt/Sim domain. (**b**) Induction of chromatin condensation in DMEM-cultured PC12 cells with expression of IPAS WT, IPAS C and IPAS C2. PC12 cells were transfected with pEGFP–IPAS constructs, stained with MitoRed and Hoechst 33342 and observed using a fluorescence microscope. Two representative images of cells expressing IPAS WT, C and C2 were shown. Arrowheads show the cells with mitochondrial localization of IPAS, mitochondria clustering and chromatin condensation. (**c**) Quantification of cell death is expressed as the percentage of cells displaying nuclear condensation. Cells were transfected and stained as shown in (**b**). A minimum of 100 cells per sample was counted. Data shown in the bar graph are averages ± S.D. of three independent experiments. **$P < 0.01$ for indicated comparison

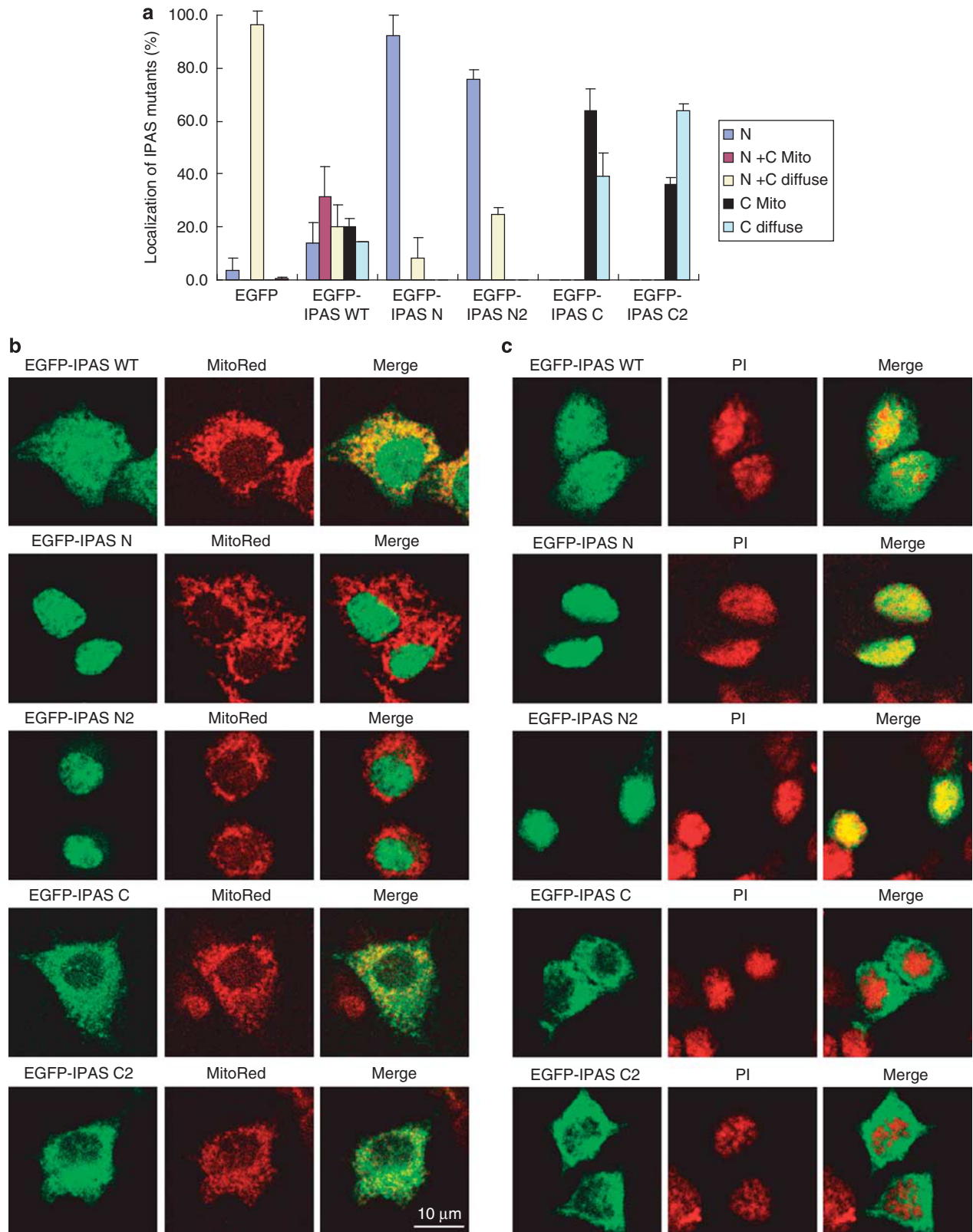**Figure 4** Subcellular localization of IPAS WT and its deletion mutants in PC12 cells. (**a**) PC12 cells were transfected with pEGFP–IPAS constructs, incubated with Z-VAD-FMK, stained with MitoRed and counted the percentage of cells showing different localization of IPAS mutants. Data shown in the bar graphs are averages ± S.D. of three independent experiments. N, Nucleus; C, cytoplasm; Mito, mitochondria. (**b** and **c**) PC12 cells were transfected with pEGFP–IPAS construct, incubated with Z-VAD-FMK, stained with MitoRed (**b**) or PI (**c**) and observed using a confocal fluorescence microscope
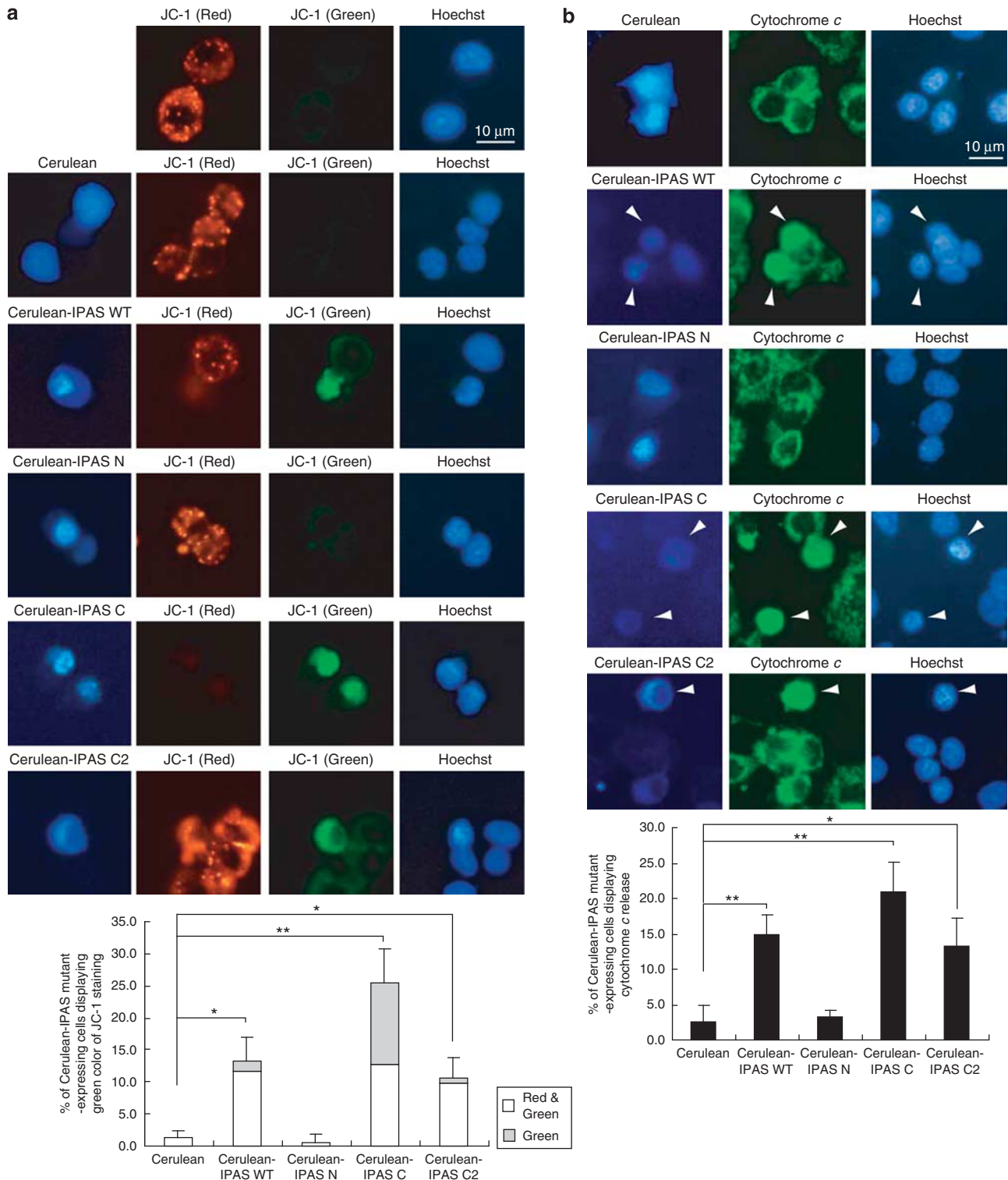
Figure 5 Induction of mitochondrial depolarization and release of cytochrome *c* by IPAS WT and its deletion mutants in PC12 cells. (**a**) Mitochondrial depolarization in DMEM-cultured PC12 cells induced by IPAS WT, IPAS C and IPAS C2. PC12 cells were transfected with pCerulean-IPAS constructs in the presence of Z-VAD-FMK and stained with JC-1 for 20 min. After washing with DMEM, the cells were observed using a fluorescence microscope. A minimum of 100 transfected cells with different staining patterns per sample was counted and the result is shown below. (**b**) Release of cytochrome *c* in DMEM-cultured PC12 cells induced by IPAS WT, IPAS C and IPAS C2. PC12 cells were transfected with pCerulean–IPAS constructs in the presence of Z-VAD-FMK and stained using an anti-cytochrome *c* antibody. A minimum of 100 cells with different staining patterns per sample was counted and the result is shown below. Data shown in bar graphs are averages ± S.D. of three independent experiments. *P<0.05 for indicated comparison. **P<0.01 for indicated comparison

was not localized in the nucleus, it was colocalized with IPAS WT in the cytoplasm. IPAS C colocalized with Bcl-x_L in the cytoplasm, particularly in the cluster of mitochondria (Figure 7f). Furthermore, we performed fluorescence resonance energy transfer (FRET) analysis between two fluorescent proteins using fluorescence lifetime imaging microscopy (FLIM) to examine the interaction between IPAS and Bcl-x_L in living cells (Figures 7g and h). Lifetimes of IPAS-Cerulean were calculated to be 1.25 and 3.18 ns, with fraction ratios of 36.3 and 63.7%, respectively (Figure 7h). The fluorescence decay of IPAS-Cerulean was considerably accelerated in the presence of Bcl-x_L-Citrine by energy transfer (Figures 7g left and h). Short and long lifetimes, τ_1 and τ_2, were reduced to 0.95 and 2.89 ns, respectively. This reduction in donor lifetimes was observed in the cytoplasm, but not in the nucleus, as shown in the FLIM map (Figure 7g bottom). On the other hand, homogeneous lifetimes were observed all over the cell when IPAS-Cerulean was expressed without Bcl-x_L-Citrine. Corresponding to the reduction of donor fluorescence lifetimes, a fluorescence rise in the decay curve of Bcl-x_L-Citrine was observed (data not shown), confirming the FRET. Similar results were obtained using a pair of IPAS-Cerulean and Citrine-Bcl-x_L (Supplementary Figure 4c). Bcl-x_L-Citrine was localized diffusely in the cytoplasm with a fraction associated with mitochondria probably because of C-terminal tag. FRET signals were detected in both cases, indicating that the interaction between IPAS and Bcl-x_L is not dependent on their cytoplasmic localization. Next, the fluorescence decay of IPAS C-Cerulean was accelerated in the presence of Bcl-x_L-Citrine by energy transfer (Figures 7g right and 7h). An N-terminal tag pair, Cerulean-Bcl-x_L and Citrine-IPAS, did not exhibit the accelerated fluorescence decay (Supplementary Figure 4d), suggesting that the distance between the N-termini of IPAS and Bcl-x_L is longer than that of the C-termini. These results demonstrate that the IPAS C-terminal domain directly binds to Bcl-x_L and strongly suggest that it can trigger a series of events leading to activation of apoptosis. To confirm this possibility, we examined whether the interaction of IPAS with Bcl-x_L inhibits the function of Bcl-x_L to bind to Bax. Immunoprecipitation assays showed that IPAS inhibited the interaction of Bcl-x_L with Bax by 60% (Figure 8a). We examined localization of endogenous Bax in PC12 cells treated with CoCl$_2$. Figure 8b shows that Bax is predominantly cytosolic in resting cells and translocates into membrane fractions in response to CoCl$_2$ treatment. Furthermore, we examined the effect of IPAS/HIF-3α siRNA treatment on binding of Bcl-x_L with Bax in PC12 cells. Figure 8c shows that Bcl-x_L formed a complex with Bax in resting cells and stimulation with CoCl$_2$ resulted in the complete dissociation of the complex. IPAS/HIF-3α siRNA treatment inhibited this dissociation, suggesting that endogenous IPAS enhanced the dissociation of Bcl-x_L/Bax complex in CoCl$_2$-treated cells. Finally, we examined whether ectopic expression of Bcl-x_L inhibits IPAS-mediated activation of caspase-3. As shown in Figure 8d, Bcl-x_L strongly inhibited the activation of caspase-3. Bcl-2 inhibited this activation to some extent, probably because Bcl-2 weakly bound to IPAS and/or strongly bound to free Bax.
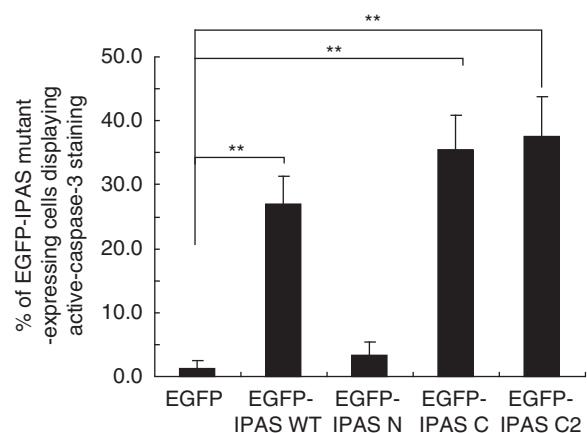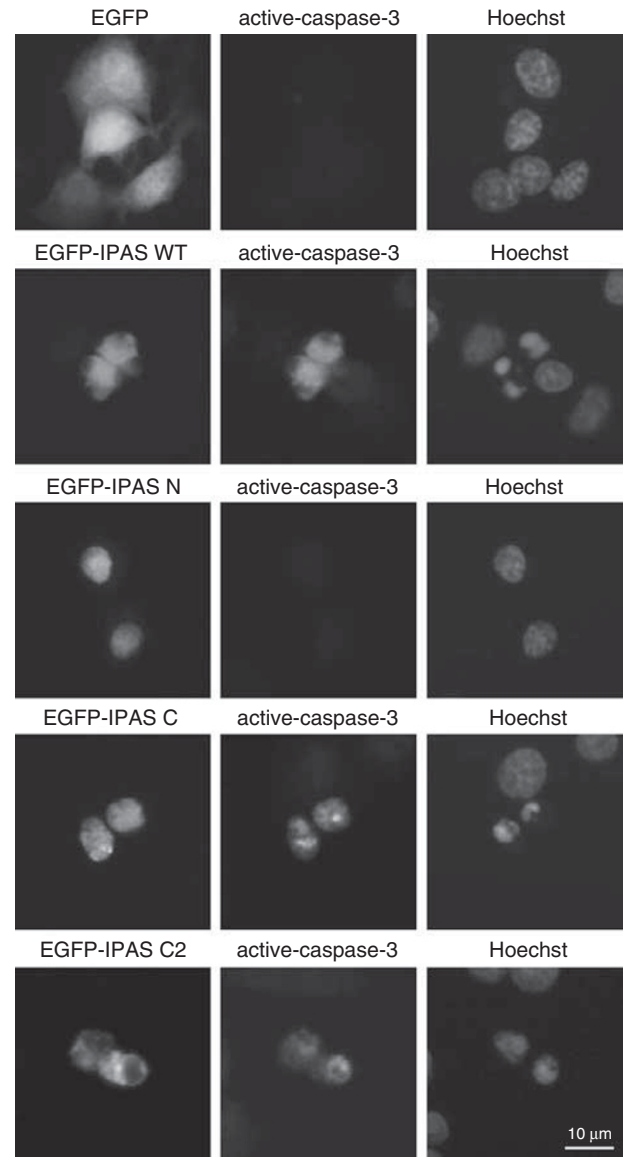
Figure 6 Activation of caspase-3 by IPAS WT, IPAS C and IPAS C2. PC12 cells were transfected with pEGFP–IPAS constructs and stained with active-caspase-3 antibody and Hoechst 33342. A minimum of 100 transfected cells showing different staining patterns per sample was counted and the result is shown below. Data shown in bar graphs are averages ± S.D. of three independent experiments. **$P < 0.01$ for indicated comparison

Binding of IPAS to HIF-1α and HLF. IPAS was originally identified as a negative regulator of HIF-1-mediated hypoxic response and is reported to directly bind to HIF-1α and HLF.[4] We examined whether our IPAS constructs bind to HIF-1α and HLF. As expected, IPAS WT and IPAS N bound to HIF-1α and HLF in the co-immunoprecipitation assay (Supplementary Figures 5a and 6a). IPAS C also interacted with HIF-1α and HLF, with an intensity similar to IPAS N. When co-expressed with HIF-1α or HLF, most of the IPAS WT was colocalized with HIF-1α and HLF in the nucleus, particularly in the nuclear speckles (Supplementary Figures 5b and 6b). Similar colocalization of IPAS N with HIF-1α and HLF was observed in the nuclear speckles. Unexpectedly, HIF-1α and HLF were colocalized with IPAS C in the clusters of mitochondria. Binding affinity between IPAS WT and HIF-1α was compared with that between IPAS WT and Bcl-x$_L$. IPAS WT bound to both Bcl-x$_L$ and HIF-1α, suggesting that similar affinity was present between the two interactions (Supplementary Figure 7). On the other hand, binding of IPAS C to HIF-1α was not observed when Bcl-x$_L$ was co-expressed. Similar results were obtained when HLF was used instead of HIF-1α. These results demonstrate that IPAS binds to HIF-1α and HLF using both the N-terminal and C-terminal regions and that the C-terminal region of IPAS has two functional regions. One acts as a region for binding to Bcl-x$_L$ and the other a region for binding to HIF-1α and HLF.

Discussion

Helix-loop-helix and PAS A domains that function as dimerization domains are localized in the N-terminal region of IPAS. On the other hand, no noticeable domains were reported in the C-terminal region. We determined that a specific sequence that is involved in the induction of apoptosis is localized in the C-terminal region, especially in the most C-terminal part. C-terminal 67 amino acids used for IPAS C2 constructs are encoded by exon 16 (final exon) and this exon is not used in other splicing variants of HIF-3α,[5] suggesting that other splicing variants may have no pro-apoptotic activity. Figure 8e shows our present model for the action of IPAS on apoptosis. IPAS was able to bind to some of pro-survival Bcl-2 members, such as Bcl-x$_L$ through the C-terminal region on the mitochondria and may block the interaction between Bcl-x$_L$ and Bax, thus activating a Bax-dependent apoptotic cascade, followed by release of cytochrome *c* and activation of caspase-3. This study shows that the C-terminal region of IPAS is responsible for binding to Bcl-x$_L$. Observations that interaction between Bcl-x$_L$ and Bax was decreased by overexpression of IPAS and increased by knockdown of IPAS support the model (Figures 8a and c). Finding that endogenous Bax was translocated to membrane fractions in response to CoCl$_2$ treatment (Figure 8b) also supports the model. The mode of action of IPAS is reminiscent of BH3 only proteins. We surveyed sequences analogous to the BH3 domain within the C-terminal region, and found a region with very weak similarity to the BH3 domain. However, introduction of point mutations in the sequence did not inhibit the binding to Bcl-x$_L$, suggesting that the binding mode of IPAS to pro-survival Bcl-2 members may be different from that of BH3 only proteins.

Preferential binding of IPAS to Bcl-x$_L$, Bcl-w and Mcl-1, but not Bcl-2 and A1 may be dependent on the distinctive binding mode of IPAS to pro-survival Bcl-2 members. Further experiments are required to characterize key sequences within IPAS necessary for binding to pro-survival Bcl-2 members.

Though we focused on the interaction of Bcl-x$_L$ with Bax, Bcl-x$_L$ is also known to bind to and inhibit activation of Apaf-1, a transmitter of apoptotic signals from mitochondrial damage to activate caspases.[24] IPAS may also inhibit binding of Bcl-x$_L$ to Apaf-1 and other interacting proteins. Bcl-x$_L$ is critical for the survival of immature neurons, whereas Bax and Apaf-1 are crucial for neuronal cell death in the nervous system.[25] Therefore, the functions of IPAS associated with these proteins may be important for neuronal cell death *in vivo*. We observed that IPAS was induced in the brain including substantia nigra and locus ceruleus in response to CoCl$_2$, suggesting that IPAS expression may be related to neuronal cell death occurring in Parkinson's disease and other neurodegenerative diseases. ROS seems to contain the driving force for neurodegeneration in Parkinson's disease.[15,26] It is known that IPAS is predominantly expressed in the Purkinje cells of the cerebellum.[4] However, it seems that these cells, despite IPAS expression, do not undergo apoptosis. One possible reason is that post-translational modification of IPAS occurs to avoid cell death in these cells. Although evidence for the modification of IPAS is presently not found, there are multiple consensus phosphorylation sites recognized by signal-regulated protein kinases in the IPAS sequence. This study demonstrates that IPAS was localized in nucleus rather than cytoplasm in HEK293T cells, and almost all IPAS was translocated to the nucleus when expressed with HIF-1α and HLF. Possible inhibitory proteins that interact with IPAS may forcibly sequester IPAS in the nucleus or other organelles to suppress its pro-apoptotic activity.

We confirmed that IPAS forms a complex with HIF-1α and HLF. The N-terminal region of IPAS exhibited binding activity to HIF-1α and HLF. It is plausible to assume that this association occurs through the bHLH (basic helix-loop-helix) and PAS domains present in the N-terminal region since the domains are used for a common dimerization interface in bHLH-PAS proteins. However, association of the C-terminal region with HIF-1α and HLF was unexpected. We believe that HIF-1α and HLF were accumulated in the mitochondria through a part of the IPAS C-terminal region (Supplementary Figures 6 and 7). Known-sequence motifs serving as protein interaction were not found in the region by a computer database search. It is necessary to delineate the regions that contributed to the binding in both the IPAS C-terminal region and the HIF-1α/HLF sequences.
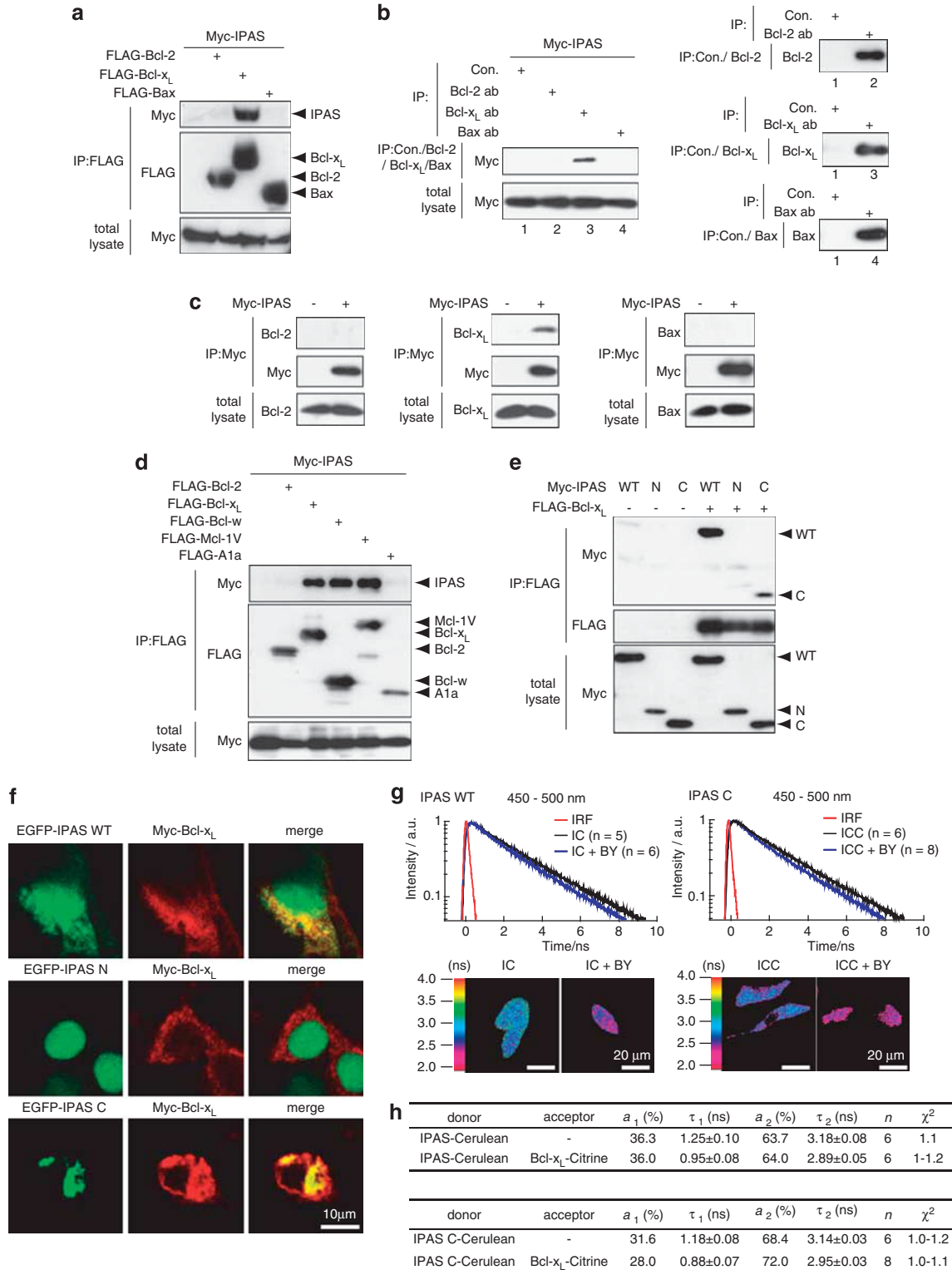
Molecular mechanisms for switching from transcription factor to pro-apoptotic protein and vice versa are presently unknown, and elucidation of the mechanism will be needed for understanding of ROS-induced cell death.

RPMI-1640 (Wako Pure Chemical Industries, Osaka, Japan) supplemented with 10% fetal bovine serum in collagen IV-coated dishes (BD Biosciences, San Jose, CA, USA) under 5% CO_2 at 37 °C, and transferred every three days. HEK293T cells and CHO-K1 cells were maintained as described.[27,28] PC12 and CHO-K1 cells were transfected using Lipofectamine 2000 (Invitrogen, Carlsbad, CA, USA) according to the manufacturer's protocol. HEK293T cells were transfected using Lipofectamine 2000 and as described.[27,29]

Cell viability assay with trypan blue dye exclusion. Cell number and viability were determined with a conventional hemocytometer by trypan blue dye exclusion. PC12 cells were plated in 6-well plate at 1.4×10^6 cells per well. After incubation for 24 h, cells were treated with 100 or 150 μM $CoCl_2$ for 24 h in the indicated medium, and collected with 5 mM EDTA in Hank's balanced salt solution (Invitrogen).

donor	acceptor	a_1 (%)	τ_1 (ns)	a_2 (%)	τ_2 (ns)	n	χ^2
IPAS-Cerulean	-	36.3	1.25±0.10	63.7	3.18±0.08	6	1.1
IPAS-Cerulean	Bcl-x$_L$-Citrine	36.0	0.95±0.08	64.0	2.89±0.05	6	1-1.2

donor	acceptor	a_1 (%)	τ_1 (ns)	a_2 (%)	τ_2 (ns)	n	χ^2
IPAS C-Cerulean	-	31.6	1.18±0.08	68.4	3.14±0.03	6	1.0-1.2
IPAS C-Cerulean	Bcl-x$_L$-Citrine	28.0	0.88±0.07	72.0	2.95±0.03	8	1.0-1.1

Determination of DNA fragmentation. PC12 cells were plated in collagen IV-coated 60 mm dish at 4×10^6 cells per dish. After incubation for 24 h, cells were treated with 150 μM CoCl$_2$ for 16 h in the indicated medium, collected and lysed in 100 μl of lysis buffer (10 mM Tris-HCl, pH 7.4, 10 mM EDTA and 1% Triton X-100). After centrifugation at $1100 \times g$ for 10 min, DNA was extracted from the supernatant and analyzed by agarose gel electrophoresis.

Nuclear staining with Hoechst 33342. PC12 cells were treated with 150 μM CoCl$_2$ for 16 h in the indicated medium, stained with Hoechst 33342 for 30 min, fixed in 4% paraformaldehyde-PBS and mounted with Mowiol (Calbiochem, San Diego, CA, USA).

Annexin V/PI staining. Annexin V-FITC Apoptosis detection kit was purchased from B-bridge (San Jose, CA, USA). PC12 cells on glass coverslips were treated with or without 150 μM CoCl$_2$ for 16 h in the indicated medium. The assays were carried out according to the manufacturer's protocol. Cells were mounted in Mowiol and examined using a fluorescence microscope (Olympus IX71, Olympus, Tokyo, Japan). Caspase inhibitor, Z-VAD-FMK was purchased from Medical Biological Laboratories (Nagoya, Japan).

RT-PCR. PC12 cells were treated with or without 150 μM CoCl$_2$ for 6 or 10 h in the indicated medium. Total RNA was extracted from cells using RNAiso (Takara Bio, Otsu, Japan). cDNAs were synthesized using oligo random hexamers (Invitrogen) and ReverTra Ace transcriptase (Toyobo, Osaka, Japan). A fraction (1 μl) of synthesized cDNA was amplified in a 20 μl reaction mixture containing 5 units of Ex Taq HS polymerase (Takara Bio). PCR cycles were chosen within the linear range of amplification. The PCR procedure consisted of 16 cycles of reaction for 18 S rRNA cDNA, 35 for IPAS and HIF-3α: 94 °C for 30 s, 60 °C for 30 s and 72 °C for 20 s. The primers used for the reaction were described previously.[23]

siRNA. RNA oligonucleotides (21 nucleotides) homologous to mouse/rat HIF-3α/ IPAS were designed as follows. Forward, 5′-GCUCAUUGGACACAGUAUCU-3′; reverse, 5′-GAUACUGUGUCCAAUGAGCUU-3′. Control siRNA homologous to GFP sequence, forward, 5′-GGCUACGUCCAGGAGCGCAUU-3′; reverse, 5′-UGC GCUCCUGGACGUAGCCUU-3′. PC12 cells were treated with annealed siRNAs by using Oligofectamine or Lipofectamine 2000 (Invitrogen) according to the manufacturer's protocol. At 24 h after transfection, cells were treated in the indicated medium with 150 μM CoCl$_2$ for indicated times.

Molecular cloning and plasmid construction. Mouse IPAS cDNA was kindly provided by Dr. Y. Makino. All IPAS cDNA fragments were prepared by PCR and ligated into pEF-BOS vector containing three Myc tags, pEGFP-C1 vector or pCerulean-C1 vector. The full-length cDNAs of mouse Bcl-2, Bcl-x$_L$, Bcl-w and Bax were synthesized by PCR using mouse brain cDNA derived from C57BL6J as a template. Mouse Mcl-1V and A1a were synthesized using mouse lung cDNA. Mcl-1V is a splicing variant of Mcl-1 and lacks 46 amino acids residues within Mcl-1. These cDNAs were ligated into the pEF-BOS vectors containing three Myc, three FLAG or an HA tag. pBOS-FLAG human HIF-1α and pBOS-FLAG mouse HLF were described previously.[30] The full-length cDNAs of HIF-1α and HLF were ligated into the pCitrine-C1 vector. All tags were added to the N-terminus of each protein. For FLIM-FRET analysis, IPAS, IPAS C and Bcl-x$_L$ were ligated into the pCerulean-N1

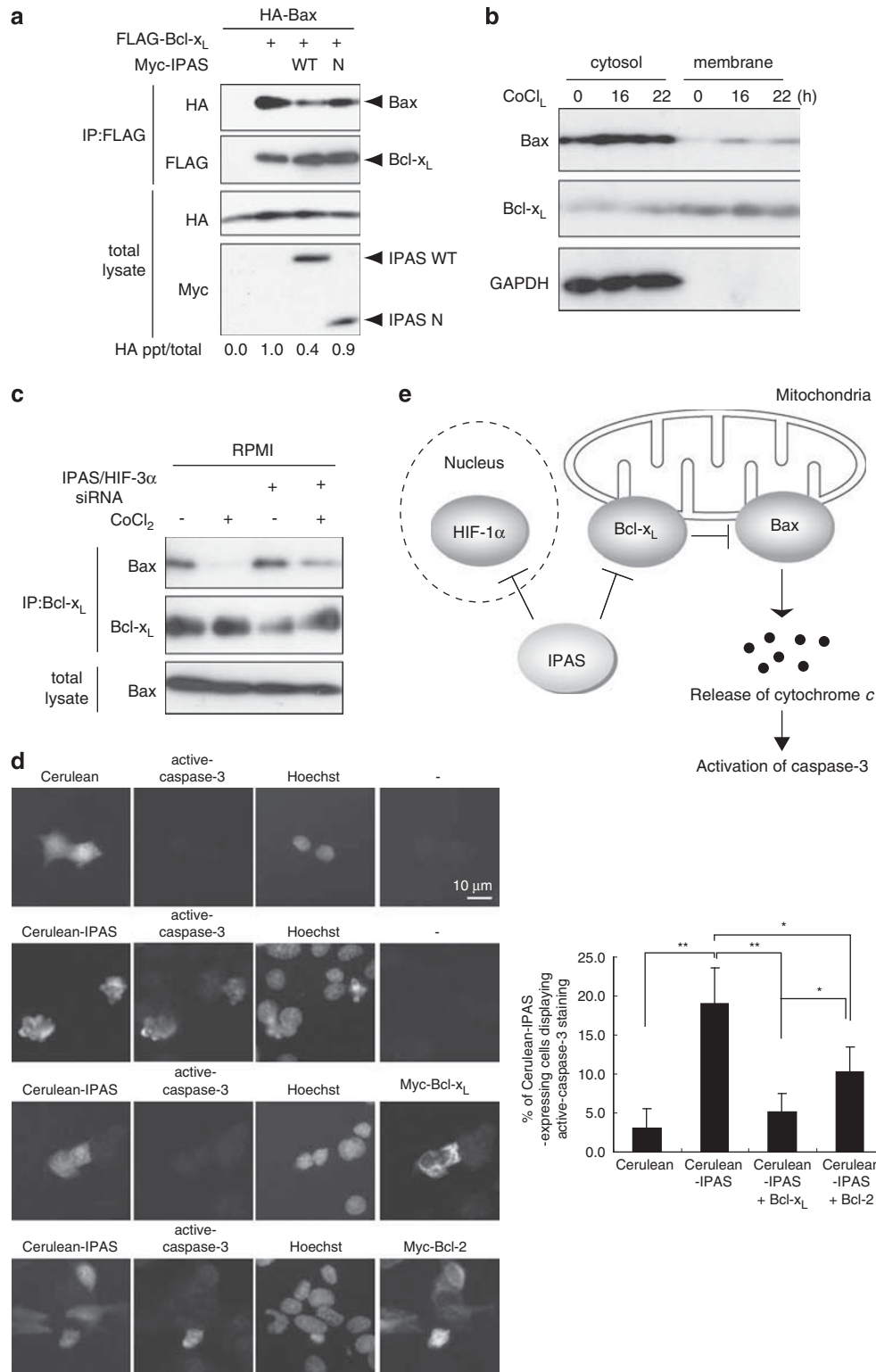and pCitrine-N1 vector for a C-terminal tag, and pCerulean-C1 and pCitrine-C1 for an N-terminal tag.

Immunostaining. After fixation by 4% paraformaldehyde-PBS solution and permeabilization with 0.5% (or 0.1% for anti-cytochrome *c*) Triton X-100 in PBS for 5 min, cells were incubated with indicated primary antibodies at room temperature for 1 h, and then with the appropriate secondary antibodies at room temperature for 1 h. Cells were finally mounted in Mowiol and examined using a laser scanning confocal microscope (Olympus FV300) or a fluorescence microscope (Olympus IX71). An antibody against cytochrome *c* and active-caspase-3 was purchased from BD Pharmingen (San Jose, CA, USA) and Promega (Fitchburg, WI, USA), respectively. In PI staining, cells were treated by 100 μg/ml RNase at 37 °C for 20 min after fixation by 4% paraformaldehyde-PBS solution, and incubated by 400 ng/ml PI for 10 min.

Determination of mitochondrial transmembrane potential with JC-1. PC12 cells were transfected with indicated constructs and treated with Z-VAD-FMK. 24 h after transfection, cells were incubated with JC-1 (Cayman Chemical, Ann Arbor, MI, USA) and Hoechst 33342 for 20 min at 37 °C, and observed by using a fluorescence microscope (Olympus IX71).

Immunoprecipitation and immunoblotting. Immunoprecipitation assays were carried out as described previously.[31] Cells were lysed in lysis buffer containing 20 mM Hepes (pH7.5), 100 mM NaCl, 1.5 mM MgCl$_2$, 1 mM EGDA, 10 mM Na$_2$P$_2$O$_7$, 10% glycerol, 1% Nonidet P-40, 1 mM dithiothreitol, 1 mM Na$_3$VO$_4$, 1 mM PMSF and 1% Aprotinin (Sigma, St. Louis, MO, USA). For Bax-Bcl-x$_L$ binding assay, cells were lysed in CHAPS buffer (PBS (pH 7.4) containing 10 mM CHAPS, 150 mM NaCl, 1 mM NaF, 10 mM Na-phosphate, 1 mM dithiothreitol, 1 mM Na$_3$VO$_4$, 1 mM PMSF and 1% Aprotinin) for 1 h on ice and centrifuged at $12\,000 \times g$. The anti-Bcl-x$_L$ antibody was added to the supernatant of the CHAPS lysate and immunoprecipitates were analyzed. Binding reaction mixtures were loaded on $10 \sim 13\%$ SDS-polyacrylamide gels. After electrophoresis, the proteins were blotted onto a nitrocellulose membrane (GE Healthcare, Little Chalfont, UK) and probed with indicated first antibodies. Anti-Bcl-2 was purchased from Santa Cruz (Santa Cruz, CA, USA). Anti-Bcl-x$_L$, anti-Bax and anti-caspase-3 antibodies were purchased from Cell Signaling Technology (Danvers, MA, USA). Anti-Myc and anti-HA antibodies were purchased from Medical Biological Laboratories. Anti-FLAG and anti-β-tubulin was from Sigma. Horseradish peroxidase-linked goat anti-rabbit IgG (Jackson ImmunoReseach, West Grove, PA, USA) was used as the second antibody. The membrane was developed with the ECL Plus detection system (GE Healthcare).

FLIM measurements. FLIM measurements were carried out as described previously.[28] In brief, fluorescence lifetimes of cells were measured on an inverted microscope (Zeiss (Jena, Germany): Axiovert 135, $\times$ 100 oil immersion objective with numerical aperture of 1.3) equipped with a disk anode microchannel plate photomultiplier (Europhoton, Berlin, Germany), which can detect photons in a time-resolved and space-resolved manner by using a time-correlated single-photon-counting technique. Fluorescence from live cell samples incubated at 37 °C was sequentially collected at 475 ± 25 nm for Cerulean and 575 ± 25 nm for Citrine by bandpass filters at a count rate below about 0.5 counts (pixel · s)$^{-1}$.

Figure 7 Binding of IPAS to pro-survival Bcl-2 family members through its C-terminal region. (**a**) Binding of IPAS to Bcl-x$_L$ but not to Bcl-2 and Bax. HEK293T cells were transfected with indicated combinations of expression plasmids and analyzed by immunoprecipitation with antibody against FLAG followed by immunoblotting with antibody against Myc. (**b** and **c**) Binding of IPAS to endogenous Bcl-x$_L$ but not to Bcl-2 and Bax. HEK293T cells were transfected with pBOS–3Myc–IPAS, incubated in the presence of Z-VAD-FMK and cell lysates were analyzed by immunoprecipitation with antibodies against rabbit IgG (Con.), Bcl-2, Bcl-x$_L$ and Bax followed by immunoblotting with antibody against Myc (**b**), or analyzed by immunoprecipitation with an antibody against Myc followed by immunoblotting with antibodies against Bcl-2, Bcl-x$_L$ and Bax (**c**). (**d**) Binding of IPAS to pro-survival Bcl-2 family members. Assays were carried out as in (**a**). (**e**) Binding of IPAS to Bcl-x$_L$ through its C-terminal region. Assays were carried out as in (**a**). (**f**) Subcellular localization of IPAS and Bcl-x$_L$ in HEK293T cells. HEK293T cells were transfected with pEGFP–IPAS constructs together with pBOS–3Myc–Bcl-x$_L$ plasmid, stained with antibody against Myc and observed using a confocal fluorescence microscope. (**g**) FLIM-FRET analysis of the interaction between IPAS-Cerulean (IC) and Bcl-x$_L$-Citrine (BY) (left) and between IPAS C-Cerulean (ICC) and Bcl-x$_L$-Citrine (right) in living CHO-K1 cells. CHO-K1 cells were transfected with indicated combinations of expression plasmids. The fluorescence decay curves of Cerulean (blue) represent an average of fluorescence decay data obtained from the cytoplasmic area of the observed cells. The decay curve of separately expressed IPAS-Cerulean or IPAS C-Cerulean (shown in black) was also shown. The shapes of the recorded instrumental response function (IRF) are shown in red. Data shown are representative of three independent experiments (top). FLIM images in the presence (IC + BY) or (ICC + BY) or absence (IC) or (ICC) of Bcl-x$_L$-Citrine. Lifetime maps were made from TSCSPC data by fitting data to a single exponential decay. In the FLIM map, color corresponds to the fluorescence lifetime indicated by a false color scale (bottom). (**h**) Fluorescence decay data for IPAS-Cerulean or IPAS C-Cerulean in the presence or absence of Bcl-x$_L$-Citrine in living CHO-K1 cells. a_1 and a_2 are the exponential coefficients for the $\tau 1$ and $\tau 2$ decay times, respectively. *n*: number of cells examined. The differences between the two $\tau 1$ values and the two $\tau 2$ values in the both case of IPAS WT and IPAS C were significant ($P < 0.001$)

a

HA-Bax

b

c

d

e

Subcellular fractionation. PC12 cells were lysed in lysis buffer containing 20 mM Hepes (pH7.5), 100 mM NaCl, 1.5 mM MgCl₂, 1 mM EGDA, 10 mM Na₂P₂O₇, 10% glycerol, 1 mM dithiothreitol, 1 mM Na₃VO₄, 1 mM PMSF and 1% Aprotinin. Cell lysates were vortexed for 15 s and centrifuged at 16 000 × *g* for 20 min. Pellets contained the enriched mitochondrial fraction, whereas supernatants contained mainly the cytosolic fractions. Pellets were re-lysed into lysis buffer shown above with Nonidet P-40. 20 μg of proteins were analyzed by immunoblotting with antibodies against Bax, Bcl-xL and GAPDH (Trevigen, Gaithersburg, MD, USA).

Statistical analysis. Data are given as mean ± standard deviation, with the number of the experiments indicated. Statistical significance was established by Student's *t* tests.

Figure 8 Inhibition of the Bcl-x$_L$/Bax complex formation by IPAS. (**a**) Inhibition of interaction between Bcl-x$_L$ and Bax by IPAS. HEK293T cells were transfected with indicated combinations of expression plasmids, incubated in the presence of Z-VAD-FMK and analyzed by immunoprecipitation with antibody against FLAG followed by immunoblotting with antibody against HA. Immunoprecipitated HA-Bax was normalized to total HA-Bax in the lysates in each lane and the result is shown below. (**b**) Western blot analysis of subcellular localization of endogenous Bax in PC12 cells. Cells were treated with CoCl$_2$ for indicated times and separated into cytosolic and membrane fractions, followed by immunoblotting with indicated antibodies. Bcl-x$_L$ and GAPDH were controls for cytosol and mitochondrial localization, respectively. (**c**) Inhibition of dissociation of the Bcl-x$_L$/Bax complex by IPAS/HIF-3α siRNA treatment. PC12 cells were transfected with GFP or IPAS/HIF-3α siRNA and incubated with or without CoCl$_2$ in the presence of Z-VAD-FMK for 16 h, and cell lysates were analyzed by immunoprecipitation with antibody against Bcl-x$_L$ followed by immunoblotting with antibody against Bax. (**d**) Inhibition of IPAS-induced activation of caspase-3 by Bcl-2 family members. PC12 cells were transfected with pCerulean, pCerulean-IPAS, pCerulean-IPAS + pBOS-3MycBcl-x$_L$ and pCerulean-IPAS + pBOS-3MycBcl-2, respectively, stained with active-caspase-3 antibody and Hoechst 33342 and observed using a fluorescence microscope. A minimum of 100 transfected cells with or without active caspase-3 staining per sample was counted and the result is shown at right. Data shown in bar graphs are averages ± S.D. of three independent experiments. *$P < 0.05$ for indicated comparison. **$P < 0.01$ for indicated comparison. (**e**) A model for the action of IPAS in apoptosis. IPAS is bound to Bcl-x$_L$ and some other pro-survival Bcl-2 members on mitochondria and blocks the interaction of Bcl-x$_L$ with Bax, thus activating the pro-apoptotic function of Bax, followed by release of cytochrome c and activation of caspase-3. IPAS functions as a dual function protein involved in transcription repression of HIF-1α and apoptosis

Conflict of Interest

The authors declare no conflict of interest.

1. Hirota K, Semenza GL. Regulation of hypoxia-inducible factor 1 by prolyl and asparaginyl hydroxylases. *Biochem Biophys Res Commun* 2005; **338**: 610–616.
2. Kaelin Jr WG. The von Hippel-Lindau protein, HIF hydroxylation, and oxygen sensing. *Biochem Biophys Res Commun* 2005; **338**: 627–638.
3. Schofield CJ, Ratcliffe PJ. Signalling hypoxia by HIF hydroxylases. *Biochem Biophys Res Commun* 2005; **338**: 617–626.
4. Makino Y, Cao R, Svensson K, Bertilsson G, Asman M, Tanaka H et al. Inhibitory PAS domain protein is a negative regulator of hypoxia-inducible gene expression. *Nature* 2001; **414**: 550–554.
5. Makino Y, Uenishi R, Okamoto K, Isoe T, Hosono O, Tanaka H et al. Transcriptional up-regulation of inhibitory PAS domain protein gene expression by hypoxia-inducible factor 1 (HIF-1): a negative feedback regulatory circuit in HIF-1-mediated signaling in hypoxic cells. *J Biol Chem* 2007; **282**: 14073–14082.
6. Carmeliet P, Dor Y, Herbert JM, Fukumura D, Brusselmans K, Dewerchin M et al. Role of HIF-1alpha in hypoxia-mediated apoptosis, cell proliferation and tumour angiogenesis. *Nature* 1998; **394**: 485–490.
7. Bruick RK. Expression of the gene encoding the proapoptotic Nip3 protein is induced by hypoxia. *Proc Natl Acad Sci USA* 2000; **97**: 9082–9087.
8. Kim JY, Ahn HJ, Ryu JH, Suk K, Park JH. BH3-only protein Noxa is a mediator of hypoxic cell death induced by hypoxia-inducible factor 1alpha. *J Exp Med* 2004; **199**: 113–124.
9. Semenza GL. Targeting HIF-1 for cancer therapy. *Nat Rev Cancer* 2003; **3**: 721–732.
10. Piret JP, Minet E, Cosse JP, Ninane N, Debacq C, Raes M et al. Hypoxia-inducible factor-1-dependent overexpression of myeloid cell factor-1 protects hypoxic cells against tert-butyl hydroperoxide-induced apoptosis. *J Biol Chem* 2005; **280**: 9336–9344.
11. Chen N, Chen X, Huang R, Zeng H, Gong J, Meng W et al. BCL-xL is a target gene regulated by hypoxia-inducible factor-1 alpha. *J Biol Chem* 2009; **284**: 10004–10012.
12. Xu W, Chi L, Row BW, Xu R, Ke Y, Xu B et al. Increased oxidative stress is associated with chronic intermittent hypoxia-mediated brain cortical neuronal cell apoptosis in a mouse model of sleep apnea. *Neuroscience* 2004; **126**: 313–323.
13. Fujimura M, Tominaga T, Chan PH. Neuroprotective effect of an antioxidant in ischemic brain injury: involvement of neuronal apoptosis. *Neurocrit Care* 2005; **2**: 59–66.
14. Lipton P. Ischemic cell death in brain neurons. *Physiol Rev* 1999; **79**: 1431–1568.
15. Scherz-Shouval R, Elazar Z. ROS, mitochondria and the regulation of autophagy. *Trends Cell Biol* 2007; **17**: 422–427.
16. Wang G, Hazra TK, Mitra S, Lee HM, Englander EW. Mitochondrial DNA damage and a hypoxic response are induced by CoCl2 in rat neuronal PC12 cells. *Nucleic Acids Res* 2000; **28**: 2135–2140.
17. Jung JY, Kim WJ. Involvement of mitochondrial- and Fas-mediated dual mechanism in CoCl2-induced apoptosis of rat PC12 cells. *Neurosci Lett* 2004; **371**: 85–90.
18. Jung JY, Han CR, Jeong YJ, Kim HJ, Lim HS, Lee KH et al. Epigallocatechin gallate inhibits nitric oxide-induced apoptosis in rat PC12 cells. *Neurosci Lett* 2007; **411**: 222–227.
19. Jung JY, Roh KH, Jeong YJ, Kim SH, Lee EJ, Kim MS et al. Estradiol protects PC12 cells against CoCl2-induced apoptosis. *Brain Res Bull* 2008; **76**: 579–585.
20. Araya J, Maruyama M, Inoue A, Fujita T, Kawahara J, Sassa K et al. Inhibition of proteasome activity is involved in cobalt-induced apoptosis of human alveolar macrophages. *Am J Physiol Lung Cell Mol Physiol* 2002; **283**: L849–L858.
21. Chachami G, Simos G, Hatziefthimiou A, Bonanou S, Molyvdas PA, Paraskeva E. Cobalt induces hypoxia-inducible factor-1alpha expression in airway smooth muscle cells by a reactive oxygen species- and PI3K-dependent mechanism. *Am J Respir Cell Mol Biol* 2004; **31**: 544–551.
22. Griguer CE, Oliva CR, Kelley EE, Giles GI, Lancaster Jr JR, Gillespie GY. Xanthine oxidase-dependent regulation of hypoxia-inducible factor in cancer cells. *Cancer Res* 2006; **66**: 2257–2263.
23. Torii S, Kobayashi K, Takahashi M, Katahira K, Goryo K, Matsushita N et al. Magnesium deficiency causes loss of response to intermittent hypoxia in paraganglion cells. *J Biol Chem* 2009; **284**: 19077–19089.
24. Hu Y, Benedict MA, Wu D, Inohara N, Nunez G. Bcl-XL interacts with Apaf-1 and inhibits Apaf-1-dependent caspase-9 activation. *Proc Natl Acad Sci USA* 1998; **95**: 4386–4391.
25. Yuan J, Yankner BA. Apoptosis in the nervous system. *Nature* 2000; **407**: 802–809.
26. Shen J, Cookson MR. Mitochondria and dopamine: new insights into recessive parkinsonism. *Neuron* 2004; **43**: 301–304.
27. Yasumoto K, Kowata Y, Yoshida A, Torii S, Sogawa K. Role of the intracellular localization of HIF-prolyl hydroxylases. *Biochim Biophys Acta* 2009; **1793**: 792–797.
28. Tomokuni Y, Goryo K, Katsura A, Torii S, Yasumoto K, Kemnitz K et al. Loose interaction between glyceraldehyde-3-phosphate dehydrogenase and phosphoglycerate kinase revealed by fluorescence resonance energy transfer-fluorescence lifetime imaging microscopy in living cells. *Febs J* 2010; **277**: 1310–1318.
29. Carpentier E, Paris S, Kamen AA, Durocher Y. Limiting factors governing protein expression following polyethylenimine-mediated gene transfer in HEK293-EBNA1 cells. *J Biotechnol* 2007; **128**: 268–280.
30. Ema M, Hirota K, Mimura J, Abe H, Yodoi J, Sogawa K et al. Molecular mechanisms of transcription activation by HLF and HIF1alpha in response to hypoxia: their stabilization and redox signal-induced interaction with CBP/p300. *Embo J* 1999; **18**: 1905–1914.
31. Torii S, Kusakabe M, Yamamoto T, Maekawa M, Nishida E. Sef is a spatial regulator for Ras/MAP kinase signaling. *Dev Cell* 2004; **7**: 33–44.

Supplementary Information accompanies the paper on Cell Death and Differentiation website (http://www.nature.com/cdd)